

Transient Transport Studies for Particle and Heat Using Tracer-Encapsulated Solid Pellet Injection in LHD

TAMURA Naoki, KHLOPENKOV Konstantin V.¹, SERGEEV Vladimir Yu.^{1,2},
KUTEEV Boris V.², SUDO Shigeru¹, MUTO Sadatsugu¹, SATO Kuninori¹,
FUNABA Hisamichi¹, INAGAKI Shigeru¹, NAGAYAMA Yoshio¹, KAWAHATA Kazuo¹
and LHD Experimental Groups I / II¹

Grad. Univ. Advanced Studies, Toki 509-5292, Japan

¹ *National Institute for Fusion Science, Toki 509-5292, Japan*

² *St. Petersburg State Polytechnical University, St. Petersburg 195251, Russia*

(Received: 11 December 2001 / Accepted: 17 June 2002)

Abstract

In order to study impurity particle transport by a transient response of the tracer ions, Tracer-Encapsulated Solid PELlet (TESPEL) has been developed. TESPEL consists of polystyrene ($-\text{CH}(\text{C}_6\text{H}_5)\text{CH}_2-$)_n as an outer shell and tracer particles as an inner core. In case of the titanium (Ti) tracer, the temporal behavior of line emissions from the highly ionized tracer ions has been clearly observed by both X-ray pulse height analyzer (PHA) and a vacuum ultra violet (VUV) spectrometer. These experimental obtained data are compared with the ones simulated by the impurity transport code, MIST. Moreover, the propagation of the cold pulse caused by TESPEL injection was observed by a 32-channel electron cyclotron emission (ECE) heterodyne radiometer and the heat plasma conductivity has been evaluated.

Keywords:

impurity transport, tracer-encapsulated solid pellet (TESPEL), diffusion coefficient, peaking factor, MIST, neutral beam injection, temperature perturbation, cold pulse propagation

1. Introduction

One of the important issues of fusion research is to understand the transport of particles and heat in magnetically confined plasma. For a better understanding of these transport mechanism, both analysis of the steady state and that of the transient state are important. Impurity injection (laser blow-off method [1], impurity pellet injection [2], etc.) is one of the common transient transport study techniques. In order to diagnose impurity transport more accurately, a tracer-encapsulated solid pellet (TESPEL) [3,4] has been developed [5] and the TESPEL injector and associated system have been installed recently on LHD [6].

TESPEL consists of polystyrene ($-\text{CH}(\text{C}_6\text{H}_5)\text{CH}_2-$)_n as an outer shell and impurity particles as an inner core. It is important that TESPEL can make a both poloidally and toroidally localized impurity particle source as a tracer, which is deposited at first within a very small volume in the plasma. Another merit of TESPEL is the easy identification of the total amount of the injected impurities due to the known size of the inner core of the TESPEL. In addition, since the TESPEL injector can inject pellets of different sizes (in a 300–950 μm range), the TESPEL penetration depth, the perturbation amplitude of the electron temperature and other

Corresponding author's e-mail: ntamura@LHD.nifs.ac.jp

parameters can be optimized according to the experimental objectives.

2. Experimental Apparatus

The Large Helical Device (LHD) [7,8] is the world's largest heliotron device (poloidal period number $l = 2$, and toroidal period number $m = 10$) with a major radius $R = 3.50\text{--}4.05$ m, average minor radius $a = 0.6$ m, magnetic field up to 3 T generated by superconducting coils. The TESPEL injector has been installed on LHD Port #3-O and a TESPEL is injected from the outboard side by means of the pneumatic pipe-gun technique. The accelerating gas is Helium and its pressure is 30 atm. The obtained TESPEL velocity is typically in the range of 250–400 m/sec. The 59 TESPELs can be loaded in the rotating disk. The ablation light of TESPEL injected into LHD plasma is observed by the CCD cameras and the photo-multiplier tubes (PMT). These are equipped with the corresponding interference filters for shell and tracer. By using the known TESPEL velocity, the high time-resolved PMT signal is translated to the TESPEL position in the plasma. Thus, the location and width of the tracer deposition can be measured.

In the case of an impurity transport study, titanium (Ti) was used as a tracer. The typical shell diameter for this study is about 700 μm and several Ti micro-balls (with 80–100 μm diameter) have been filled inside the TESPEL. The total amount of Ti particle was varied approximately in the $(0.5\text{--}3) \times 10^{17}$ range.

In experiments, the temporal and spatial behaviors of the electron density (n_e) are measured by a 10 channel FIR laser interferometer [9]. The time evolution of the electron temperature (T_e) is measured by an ECE heterodyne radiometer [10] with a high time resolution. The T_e profile is also measured with a good spatial (~ 2 cm) resolution by multi-point Thomson scattering [11]. The behavior of the Ti line emissions is measured by an X-ray pulse height analyzer (PHA) [12] and a vacuum ultra violet (VUV) spectrometer. Two PHA systems have been used. One system (PHA2O) is installed on the equatorial plane of LHD Port #2-O to observe the LHD plasma center. Another (PHARD) system located at Port #2.5-L has 3 channels to observe the radial profile of X-ray emissions. The energy resolution of the PHA systems is approximately 300 – 400 eV. Therefore, the measured Ti $K\alpha$ emission by the PHA systems contains Ti $K\alpha$ line emissions from several charge states (He-like, Li-like, Be-like, etc.).

3. Impurity Tracer Injection Experiments

There have been few studies on impurity transport in stellarator type devices, while many experiments for impurity transport have been performed in tokamaks. Several important results were obtained in Heliotron E plasmas heated by neutral beam injection (NBI) [13]. It was observed that the diffusivity has an important role on the impurity transport in NBI plasmas, while the inward flow plays only a minor role. However, this experiment was performed only with a co-NBI plasma setup. Thus, it is still an important task to investigate whether the difference of the NBI direction can cause a significant difference of the impurity transport as observed in tokamaks.

The impurity transport in NBI plasmas with various NBI directions is studied in LHD by means of the TESPEL injection. Figure 1 shows an example of the time evolutions of Ti $K\alpha$ emission measured by PHA2O and Ti XIX ($\lambda = 169.6$ Å) measured by VUV spectrometer in LHD shot #27864. In this shot, TESPEL was injected at $t \sim 1.190$ sec during co-NBI. The Ti $K\alpha$ emission rises to its maximum, during approximately 500 ms after the injection and the emission decay time is estimated as 1.48 sec between the time when the Ti $K\alpha$ emission reaches a maximum value and the time when NBI was switched off. The profiles of n_e and T_e before and after TESPEL injection and their temporal evolutions are shown in Fig. 2. One can conclude that n_e and T_e perturbations caused by TESPEL injection can be

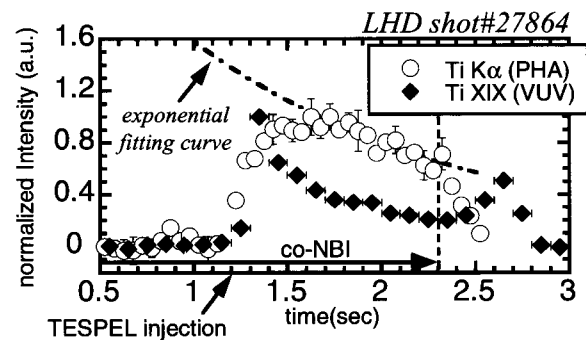


Fig. 1 An example of the temporal behavior of Ti $K\alpha$ (open circles) measured by PHA2O and Ti XIX (closed diamonds) measured by VUV spectrometer. The dash-dotted line is the exponential fitting curve for the temporal behavior of Ti $K\alpha$. Plasma condition: co-NBI plasma ($P_{\text{NBI}} = 1.7$ MW) with line averaged electron density $n_{e,\text{bar}} = 1.8 \times 10^{19} \text{ m}^{-3}$, and central electron temperature $T_e(0) \sim 2.1$ keV. NBI was terminated at $t = 2.3$ sec (vertical dashed line).

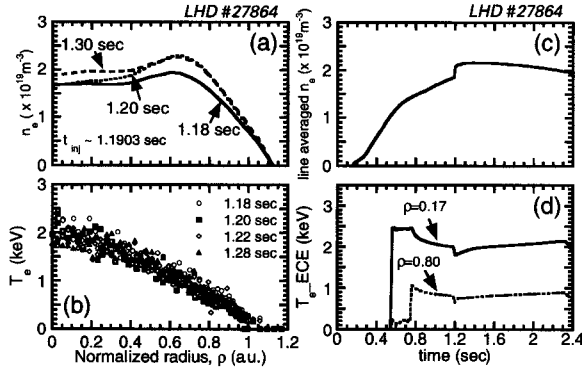


Fig. 2 Profiles of (a) n_e , (b) T_e before and after TESPEL injection and the temporal evolutions of (c) $n_{e, \text{bar}}$ (d) T_e . TESPEL injection was at $t \sim 1.1903$ sec. Same discharge as in Fig. 1.

neglected when 0.1–0.15 sec has passed since TESPEL injection. Thus, impurity transport studies were performed for times after $t = 1.3$ sec in this shot.

Simulations were done by using the impurity transport code, MIST [14]. For those, cylindrical symmetry was assumed and the radial particle flux Γ_i for the i -th charge state ion was modeled by a simple diffusive-convective model: $\Gamma_i = -D_i(r)\partial n_i/\partial r - V_i(r)n_i$, where n_i is the density of the impurity, $D_i(r)$ is the radial diffusion coefficient and $V_i(r)$ is the convective velocity, respectively. In our studies, the diffusion coefficient is assumed to be radially constant and the convective velocity term is represented as $V_i = -Cv(2rD_i/a^2)$, where Cv is the dimensionless peaking factor.

Figure 3 shows the calculated profile of Ti $K\alpha$ emission integrated along the PHARD line of sight and the experimental one for LHD #27864 at $t = 1.9$ sec before the termination of NBI. One can see from this figure that the radial profile is weakly sensitive to Cv values. Thus, only a 0–3 range of Cv could be evaluated from Fig. 3. Since this steady-state profile analysis gives only the ratio of the convective fluxes to diffusive ones, the temporally evolving data are used for further analysis. Comparison of the calculated temporal evolutions for several sets of D and Cv with the measured ones is shown in Fig. 4. A fairly good agreement is obtained with the value of $D = 900 \text{ cm}^2/\text{sec}$ and $Cv = 2$ (i.e. $V(a) = 57 \text{ cm}/\text{sec}$, where $V(a)$ is the convective velocity at the plasma edge) as a result of trial and error. From this analysis, the Ti ion transport is explained with the value of $D = (450\text{--}1800) \text{ cm}^2/\text{sec}$ and $Cv = 0\text{--}3$. Similar analysis has been performed for balanced NBI and counter-NBI plasmas with line-

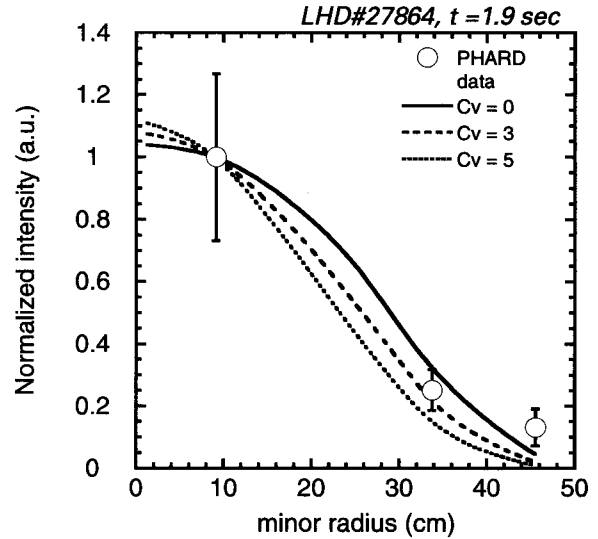


Fig. 3 Calculated profile of line-integrated Ti $K\alpha$ emission and the experimental data measured by PHARD for LHD #27864 at $t = 1.9$ sec before the termination of NBI.

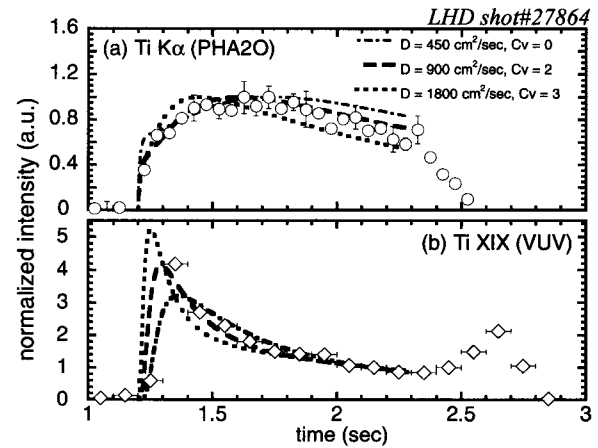


Fig. 4 Comparison of normalized temporal evolutions of the (a) Ti $K\alpha$ (open circles) and (b) Ti XIX (open diamonds) with those calculated by MIST with several sets of D and Cv (dash-dotted line: $D = 450 \text{ cm}^2/\text{sec}$, $Cv = 0$, dashed one: $D = 900 \text{ cm}^2/\text{sec}$, $Cv = 2$, dotted one: $D = 1800 \text{ cm}^2/\text{sec}$, $Cv = 3$). Calculations were stopped at $t = 2.3$ sec when the NBI was terminated. The intensity of Ti $K\alpha$ is normalized by the value at the time when the Ti $K\alpha$ emission reaches a maximum and that of Ti XIX is normalized by the value at $t = 2.15$ sec.

averaged electron density $n_{e, \text{bar}}$ in the range of $(1\text{--}2) \times 10^{19} \text{ m}^{-3}$. The pair of $D = 900 \text{ cm}^2/\text{sec}$ and $Cv = 0$ for balanced NBI case and $D = 700 \text{ cm}^2/\text{sec}$ and $Cv = 0$ for

counter-NBI case are obtained as the best fit.

In Heliotron E, no strong dependence of the impurity transport on the impurity species (Si, Fe, etc.) was observed [15]. Thus, the obtained transport coefficients by means of TESPEL with Ti tracer in LHD are compared with those by laser blow-off technique with silicon impurity in Heliotron E [13]. The D value of (700–900) cm²/sec, obtained in LHD is close to ones in Heliotron E. Small $Cv \leq 2$ values (i.e. small inward flow) for co-NBI, counter-NBI and balanced NBI plasmas obtained in LHD are also consistent with the finding for co-NBI plasmas in Heliotron E [12]. For further comparison, dependence of impurity transport coefficients on plasma parameters (electron density, NBI power and so on) should be obtained in LHD.

4. Cold Pulse Experiment

TESPEL has produced the electron temperature perturbation with small perturbations of other plasma parameters. Thus, the values of electron heat diffusivity, χ_e , in the interior of the plasma were evaluated from analysis of the cold pulse propagation caused by TESPEL injection [16]. For one, the value of χ_e was estimated as (2–5) m²/sec for the co-NBI plasma with $n_{e_bar} = 1.4 \times 10^{19}$ m⁻³ and $T_e(0) \sim 2.1$ keV. In order to obtain the χ_e for various plasma regions, the penetration depth of TESPEL should be varied. Recently, the penetration depth $\rho_{pen} = 0.87$ was obtained for the TESPEL of 336 μ m diameter, meanwhile $\rho_{pen} = 0.73$ for the TESPEL of 740 μ m. For both cases, the cold pulse propagations were clearly observed by the ECE heterodyne radiometer and could be used for further analysis.

5. Summary

TESPEL has been utilized for the transient transport studies of both impurity and heat in LHD. The effect of the NBI direction on the impurity transport was studied at the moderate range of n_{e_bar} , $(1-2) \times 10^{19}$ m⁻³. The line emissions from the Ti tracer ions were clearly observed by PHA and VUV spectrometer. The time evolutions of Ti $K\alpha$ and Ti XIX were compared with those calculated by the time dependent MIST. The diffusion coefficients D and convective velocities V , obtained for LHD plasmas with different NBI directions were compared with those obtained in Heliotron E

plasmas with co-NBI. These results in LHD were almost consistent with the findings of Heliotron E. However, in our experiment, many parameters were fixed. Thus the parametric dependencies of impurity transport on electron density, NBI power and others remain as objectives of future studies. TESPEL injection has produced the electron temperature perturbations with small perturbations of other plasma parameters. The resulting cold pulse propagations were clearly measured by an ECE heterodyne radiometer. Since the TESPEL injector can inject various sizes of TESPEL, the electron heat diffusivity, χ_e , can be studied in a widespread plasma region.

Acknowledgments

This work was supported partly by grant No. L00537 of Japan Society for the Promotion of Science.

References

- [1] E.S. Marmor *et al.*, Rev. Sci. Instrum **46**, 1149 (1975).
- [2] K. Khlopenkov *et al.*, Fusion Eng. Des. **34-35**, 337 (1997).
- [3] S. Sudo, J. Plasma Fusion Res. **69**, 1349 (1993).
- [4] S. Sudo *et al.*, Proc. of 17th IAEA Fusion Energy Conference, IAEA-CN-69/EXP/18, (Yokohama, Japan, 1998).
- [5] K. Khlopenkov *et al.*, Rev. Sci. Instrum. **69**, 3194 (1998).
- [6] N. Tamura *et al.*, J. Plasmas Fusion Res. SERIES **4**, 442 (2001).
- [7] O. Motojima *et al.*, Phys. Plasmas **6**, 1843 (1999).
- [8] M. Fujiwara *et al.*, Nucl. Fusion **40**, 1157 (2000).
- [9] K. Kawahata *et al.*, Rev. Sci. Instrum. **70**, 707 (1999).
- [10] Y. Nagayama *et al.*, Rev. Sci. Instrum. **70**, 1021 (1999).
- [11] K. Narihara *et al.*, Rev. Sci. Instrum. **72**, 1122 (2001).
- [12] S. Muto *et al.*, Rev. Sci. Instrum. **72**, 1206 (2001).
- [13] H. Kaneko *et al.*, Nucl. Fusion **27**, 1075 (1987).
- [14] R.A. Hulse, Nuclear Technology/Fusion **3**, 259 (1983).
- [15] J.E. Rice *et al.*, Nucl. Fusion **24**, 1205 (1984).
- [16] S. Inagaki *et al.*, *this conference*.